phys. stat. sol. (b) **222**, 407 (2000)

Subject classification: 61.10.Dp; 78.70.Ck

Theory of Imaging a Perfect Crystal under the Conditions of X-Ray Spherical Wave Dynamical Diffraction

V. G. KOHN (a), I. SNIGIREVA (b), and A. SNIGIREV (b)

(a) Russian Research Centre "Kurchatov Institute", 123182 Moscow, Russia

(b) European Synchrotron Radiation Facility, B.P. 220, F-38043 Grenoble, France

(Received February 25, 2000; in revised form May 19, 2000)

A theory of the formation of interference patterns due to X-ray spherical wave two-beam dynamical diffraction in a perfect crystal is presented. An asymmetrical Laue case is analyzed in detail, when a polychromatic focus is realized with different distances in front of and behind the crystal. Such a property is essential for high-energy X-rays produced by synchrotron radiation sources of the third generation because of the long distance between source and object. It is shown that a monochromatic X-ray spherical wave is focused due to dynamical diffraction when a definite relation between distances and crystal thickness is held. An X-ray beam of less than 10 μm width may be obtained. A two-dimensional intensity distribution (topograph) may be registered with a wedge-shaped crystal. It shows interference fringes of different kinds depending on crystal thickness and asymmetry rate. It is also discussed how a slit in front of the crystal influences the interference pattern. An example of an interference pattern is presented under the condition of highly asymmetrical diffraction which was obtained by a computer simulation technique. Fringes of a new kind are observed and their physical nature is discussed.

1. Introduction

Recently, a new technique was developed consisting of hard X-ray phase (refractive) contrast imaging (microscopy) of small or slightly absorbing objects. With usage of an X-ray tube or synchrotron sources up to the second generation, a single crystal collimator and analyzer are necessary to obtain resolution (see, for example, [1–4]). As for third generation synchrotron sources, it was shown that the phase contrast image may be obtained directly at some distance from the object [5–8]. In this case the uneven phase profile of the wave field is transformed into the intensity profile during propagation from the object to the detector through empty space. Moreover, a compound refractive lens for hard X-ray focusing becomes useful with third generation synchrotron sources [9–11].

The new development becomes possible due to a high level of spatial coherence of an X-ray beam either prepared by a single crystal collimator or delivered by a third generation synchrotron source. As is known, dynamical X-ray diffraction in single crystals is also realized under the condition of a coherent beam. Recently this fact was used for an estimation of spatial coherence [12].

On the other hand, we want to recall that a perfect crystal plate may focus an X-ray spherical wave under the conditions of dynamical diffraction in the Laue case. This phenomenon was predicted theoretically [13] and observed experimentally [14] more than twenty years ago. The reason is that the small transverse shift of X-rays during passage through empty space from source to crystal and from crystal to detector due to

an angular divergence becomes compensated during passage through a crystal plate of relatively small thickness much less than the external distances. This is because the possible angular width of the energy flow in the crystal under the two-beam diffraction condition is the so-called Borrmann fan that is much larger than the angular width of the incident wave which satisfies the Bragg condition. The following study [15] with a wedge shaped crystal led to the observation of an anomalous type of interference fringes compared to the fringes observed previously by Kato and Lang [16] for a range of crystal thicknesses less than the thickness of focusing.

The more complicated experimental setup containing a slit and two crystal plates was also investigated [17] both theoretically and experimentally. The coherent scattering of X-rays allows one to observe an interference pattern which depends, in general, on all elements installed in the optical scheme. Therefore in the theoretical analysis of the interference pattern it is necessary to specify in explicit form the whole experimental setup from the source to the detector. The source cross-section size and the frequency bandpass must be considered in view of the possibility to observe the coherent phenomena. In this way, any point of the source cross-section as well as any frequency value inside the frequency bandwidth can be considered as incoherent. Therefore the intensity of X-rays calculated with a point source of monochromatic radiation must be integrated over the real source cross-section size and the frequency bandwidth at any point of the interference pattern.

Up to now a detailed theoretical analysis was done for the case of symmetrical diffraction only. The experiment was made with a microfocus X-ray tube while the interference pattern was registered by a photo-sensitive film. Rather small distances of the experimental setup of about 1 m led to a small enough width of the interference pattern compared to the source cross-section size. As a result, it was impossible to observe the fine structure of the diffraction image. A synchrotron radiation source allows one to use an experimental setup with a long distance in front of the crystal and to obtain a coherent beam of a high level. In this case it is necessary to use asymmetrical diffraction to provide the polychromatic focus.

In this work a further development of the dynamical theory of X-ray spherical wave diffraction in a perfect crystal is presented. In other words, we analyze a possibility of a diffraction lens for synchrotron X-rays as well as the possible structure of interference fringes. We consider a simple experimental setup with one crystal plate where the Laue case of dynamical diffraction takes place in an asymmetrical geometry. We develop the theory in real space using a technique of propagators like in Ref. [4]. A connection of this technique with the method of plane wave expansion used in [13–15, 17] is obtained by Fourier transformation. The role of the slit between the source and the crystal is also analyzed. It is shown that under the conditions of polychromatic focusing with a wide bandpass of radiation the slit plays the role of a new incoherent source while the real source properties do not influence the interference pattern.

A specific example: the case of highly asymmetrical (804) diffraction in silicon is analyzed in detail. The result of a computer simulation of the two-dimensional interference pattern (detector position – crystal thickness) is presented. In this case the focusing phenomenon is not well pronounced. On the other hand, interference fringes of a new kind are discovered which have not been studied previously. An analytical estimation of the distance between the new fringes is made and the physical nature of the fringes is discussed.

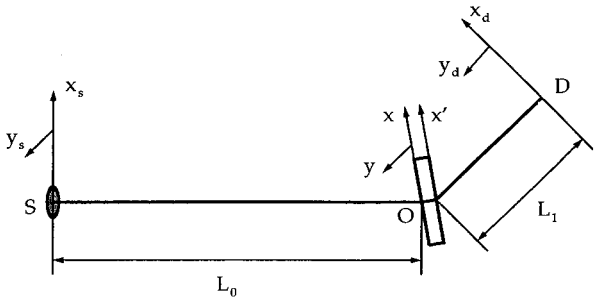

Fig. 1. Sketch of the experimental setup and the coordinate axes. S – the source, O – the perfect crystal, D – the detector

2. General Theory

2.1 Formulation in terms of propagators

The scheme of the experimental setup and the geometrical parameters are shown in Fig. 1. We consider a plane polarized wave with the polarization vector normal to the scattering plane (the plane of Fig. 1). The diffracted wave has the same polarization state. Therefore we may consider the scalar waves. The y-axes of the Cartesian coordinate system at all elements of the experimental setup is also normal to the scattering plane. We start with a spherical monochromatic wave emerging from the point x_s, y_s of the source cross-section and we consider it in the point x, y in space. The wave may be written as $\psi(\mathbf{r}, t) = \psi(\mathbf{r}, \omega) \exp(-i\omega t)$ with $\psi(\mathbf{r}, \omega) = \exp(iKr)/r$, where $K = \omega/c = 2\pi/\lambda$, c is the speed of light, $r = [z^2 + (x - x_s)^2 + (y - y_s)^2]$ where z is a longitudinal distance. The longitudinal distances of our experimental setup are much larger than the transverse distances. Therefore we may use a small angle approximation when the third and higher degrees of the ratios x/z and y/z are neglected.

We are interested in the wave field at the entrance surface of the crystal. The surface is perpendicular to the unit vector $\mathbf{n}_0$. Let the angle between z-axis and $\mathbf{n}_0$ be φ_0 (see Fig. 2). Then we introduce a notation $\gamma_0 = \cos\varphi_0$, $S_0 = \sin\varphi_0$ and write

$$\psi_0(x, y) = \exp(iKL_0 - iKxS_0]) \frac{1}{L_0} \exp\left(\frac{i\pi}{\lambda L_0} [(x\gamma_0 - x_s)^2 + (y - y_s)^2]\right). \quad (1)$$

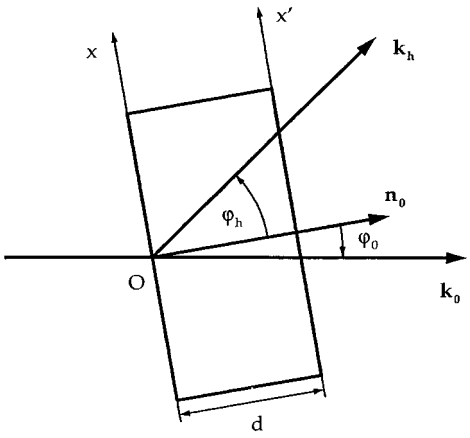

Here x is a coordinate in the entrance surface of the crystal and L_0 is the distance from the source to the crystal. The wave field (1) may be presented in the form $\exp(i\mathbf{k}_0\mathbf{r})\, E_0^{(\mathrm{in})}(x, y)$ in the local coordinate system with the origin at the point O (see Fig. 2). Here $\mathbf{k}_0$ is a wave vector having a modulus K and directed along the optical

Fig. 2. Geometrical parameters of X-ray diffraction in the crystal plate

axis SO (see Fig. 1) with the unit vector $\mathbf{s}_0$. It is easy to verify that $\mathbf{k}_0\mathbf{r} = -KxS_0$ at the entrance surface. We assume that the optical axis is chosen in such a way that the Bragg condition with the reciprocal lattice vector $\mathbf{h}$ is met accurately for the given frequency ω, namely, $(K\mathbf{s}_0 + \mathbf{h})^2 = K^2$. We also assume that the amplitude $E_0(x, y)$ is a slowly varying function compared to the exponential. Then for finding the amplitude of the diffracted wave at the exit surface of the crystal we may use the Takagi equations [18]. The wave field inside the crystal is a superposition of the transmitted and diffracted waves

$$\psi_c(x, z) = \exp(i\mathbf{k}_0\mathbf{r})E_0(x, z) + \exp(i\mathbf{k}_h\mathbf{r})\, E_h(x, z)\,, \tag{2}$$

where $\mathbf{k}_h = \mathbf{k}_0 + \mathbf{h}$ and the z-axis is chosen along the unit vector $\mathbf{n}_0$ (normal to the surface). The Takagi equations are written for the slowly varying amplitudes $E_0(x, z)$ and $E_h(x, z)$. We assume for the sake of simplicity, that the vector $\mathbf{n}_0$ lies in the scattering plane. It is necessary for extremely asymmetrical cases. The y-dependence stays the same because the perturbation of the fields occurs only in the scattering plane.

The Takagi equations are written as follows:

$$\left[\chi_0 + \frac{2i}{K}\left(-S_0\,\frac{\mathrm{d}}{\mathrm{d}x} + \gamma_0\,\frac{\mathrm{d}}{\mathrm{d}z}\right)\right] E_0(x, z) + \chi_{\bar{h}} E_h(x, z) = 0\,,$$

$$\chi_h E_0(x, z) + \left[\chi_0 + \frac{2i}{K}\left(S_h\,\frac{\mathrm{d}}{\mathrm{d}x} + \gamma_h\,\frac{\mathrm{d}}{\mathrm{d}z}\right)\right] E_h(x, z) = 0\,, \tag{3}$$

where $S_h = \sin\varphi_h$, $\gamma_h = \cos\varphi_h$, and φ_h is the angle between the diffracted wave $\mathbf{k}_h$ and $\mathbf{n}_0$ (see Fig. 2). χ_0, χ_h, and $\chi_{\bar{h}}$ are the complex coefficients of the Fourier expansion of the susceptibility of the crystal $\chi(\mathbf{r})$ with the reciprocal lattice vectors zero, $\mathbf{h}$, and $-\mathbf{h}$, correspondingly. The imaginary part of these values describes the absorption of X-rays in the crystal matter.

In the case of a single crystal of thickness d_c the solution of the Takagi equations exists in an integral form with the crystal propagators $G_{0,h}(x' - x, d_c)$ known analytically [19] (see also [20]). Thus, the wave field at the exit surface is

$$\psi_c^{(\mathrm{out})}(x', y) = \exp(i\mathbf{k}_0\mathbf{r})\, E_0^{(\mathrm{out})}(x', y) + \exp(i\mathbf{k}_h\mathbf{r})\, E_h^{(\mathrm{out})}(x', y)\,, \tag{4}$$

where $E_{0,h}^{(\mathrm{out})}(x) = E_{0,h}(x, d_c)$ and

$$E_{0,h}^{(\mathrm{out})}(x', y) = \int \mathrm{d}x\; G_{0,h}(x' - x, d_c)\, E_0^{(\mathrm{in})}(x, y)\,. \tag{5}$$

Below we are interested in the diffracted wave. Therefore we write the expression for the function $G_h(x' - x, d_c)$ only in explicit form which was taken from [20] with a simple transformation

$$G_h(x, d_c) = iC\, \exp(iA)\, \mathrm{J}_0(B\sqrt{X_0X_h})\, \theta(X_0X_h)\,, \tag{6}$$

where $\mathrm{J}_0(z)$ is the Bessel function of zeroth order, $\theta(z)$ is the Heaviside step function that equals zero for negative arguments and unity for positive arguments,

$$C = K\chi_h\,\frac{\gamma_0}{2S_B}\,, \qquad A = \frac{K\chi_0}{2S_B}\,(\gamma_h X_0 + \gamma_0 X_h)\,, \qquad B = K\sqrt{\chi_h\chi_{\bar{h}}}\,\frac{\sqrt{\gamma_0\gamma_h}}{S_B}\,,$$
$$X_0 = d_c t_h - x\,, \qquad X_h = d_c t_0 + x\,, \qquad t_0 = \tan\varphi_0\,, \qquad t_h = \tan\varphi_h. \tag{7}$$

Here $S_B = \sin 2\theta_B$ and θ_B is the Bragg angle.

At the exit surface of the crystal plate we have $\mathbf{k}_h\mathbf{r} = Kd_c\gamma_h + Kx'S_h$. To eliminate the phase $Kx'S_h$ that is quickly varying in space we need to change the direction of the optical axis behind the crystal plate as is shown in Fig. 1. Now the optical axis goes along the vector of the diffracted wave $\mathbf{k}_h$. The image (detector) plane is normal to $\mathbf{k}_h$ and has the coordinates x_d, y_d. The solution of the Maxwell wave equations in empty space behind the crystal at any distance with the known field $E_h^{(out)}(x', y)$ at the exit surface of the crystal may be written by means of the Fresnel-Kirchhoff integral relation [21] in a small angle approximation:

$$\psi(x_d, y_d) = \exp(i\Phi_1)\,\gamma_h \int dx'\,dy\, P(x_d - x'\gamma_h, L_1)\, P(y_d - y, L_1)\, E_h^{(out)}(x', y)\,, \quad (8)$$

where $\Phi_1 = KL_1 + iKd_c\gamma_h$ and

$$P(x, z) = \frac{1}{\sqrt{i\lambda z}} \exp\left(i\pi \frac{x^2}{\lambda z}\right) \quad (9)$$

is a partial propagator of the transverse wave field profile for one dimension. The factor γ_h is due to the fact that the optical axis makes an angle with the vector normal to the surface. It is easy to understand the existence of such a factor taking into account that the propagator $P(x, L_1)$ becomes the Dirac delta function $\delta(x)$ for small L_1.

The real image registered by the detector is described by the intensity distribution averaged over the source cross-section size as well as a detector resolution. The source coordinates are x_s, y_s and $\theta_\omega = (\omega - \omega_0)/\omega_0$ where ω_0 is a characteristic frequency used in the experiment. Therefore

$$I(x_d, y_d) = \int dx_s\, dy_s\, d\theta_\omega\; B(x_s, y_s, \theta_\omega)\, |\psi(x_d, y_d, x_s, y_s, \theta_\omega)|^2\,, \quad (10)$$

where $B(x_s, y_s, \theta_\omega)$ is the brightness of the source at the point x_s, y_s for a relative frequency θ_ω. The possibility to observe coherent phenomena in this approach is related to the integral over dx_s, dy_s, and $d\theta_\omega$. If the effective limits of integration are small compared to the characteristic region of smoothing of the interference fringes, then the interference fringes will be observed. The characteristic region of smoothing depends on the experimental setup. Sometimes the dependence of $|\psi|^2$ on x_s, y_s, or θ_ω may be very small or it may be completely absent.

2.2 No y-dependence

The sample disturbs only the x-dependence of the wave field. Therefore one may suppose that the image is sensitive to the x-variable only. It is easy to obtain this result taking into account the property of the propagator (9) of empty space

$$\int dx\, P(x_2 - x, z_2)\, P(x - x_1, z_1) = P(x_2 - x_1, z_1 + z_2)\,. \quad (11)$$

Indeed, the integral over y has just such a structure. Therefore we have

$$\int dy\, P(y_d - y, L_1)\, P(y - y_s, L_0) = P(y_d - y_s, L_t)\,, \quad (12)$$

where $L_t = L_0 + L_1$. Since the modulus of the propagator does not depend on $y_d - y_s$, the image becomes homogeneous along the y-axis.

However, one may use a wedge shaped crystalline sample with variable thickness along the y-axis. In this case the image will depend on $d_c(y)$ parametrically. This case is

convenient because it allows one to obtain the interference pattern for all crystal thicknesses simultaneously as a two-dimensional image. Below we shall omit the phase factors which do not influence the intensity. Also, in order to have the possibility to compare the intensity of the diffracted wave with the intensity of the initial spherical wave at the same distance, we define a relative amplitude $\tilde{\psi} = L_t \psi$. Now the image is determined by the expression

$$\tilde{\psi}(x_d, x_s) = (\lambda L_t)^{1/2} \gamma_h \int \mathrm{d}x' \, \mathrm{d}x \; P(x_d - x'\gamma_h, L_1) \, G_h(x' - x, d_c) \, P(x\gamma_0 - x_s, L_0) \,, \tag{13}$$

where the crystal thickness d_c may depend on the y-coordinate.

2.3 Polychromatic focusing

Up to now we have considered a monochromatic wave. Let us analyze what happens when the frequency of the radiation is changed by the value $\Delta\omega$. In this case we need to use another optical trajectory to satisfy the Bragg condition in the crystal. The new optical trajectory makes an angle $\Delta\theta_B = -\tan\theta_B \theta_\omega$ with the old trajectory outside the crystal plate and goes normal to the surface inside the crystal. Here, as before, $\theta_\omega = \Delta\omega/\omega$. For a small relative frequency change we may use the same long distances L_0 and L_1 as well as the same crystal propagator. However, now the centre of the diffraction region in the crystal will be shifted by the value $x_\omega = -L_0 \Delta\theta_B/\gamma_0$ as follows from Fig. 3. Taking into account an additional shift of the image behind the crystal plate, one obtains the total shift of the image in the image plane as

$$x_{d\omega} = x_\omega \gamma_h + L_1 \Delta\theta_B = (L_0/\beta - L_1) \tan\theta_B \theta_\omega \,, \tag{14}$$

where $\beta = \gamma_0/\gamma_h$ is an asymmetry factor of the X-ray diffraction.

Thus, for a small relative frequency change the main effect is a shift of the image. This shift always exists in the crystal. However, when $L_1 = L_0/\beta$, it disappears in the image plane. Therefore we obtain the same position of the image for all frequencies. We shall call this effect polychromatic focusing. The range of relative frequencies $\Delta\theta_\omega$ that may be focused is defined by the longitudinal size of the crystal plate X_c as $\Delta\theta_\omega = X_c\gamma_0/(L_0 \tan\theta_B)$. Since the Bragg angle depends on the frequency, namely, $\sin\theta_B = \pi c/(\omega d)$ where c is the speed of light and d is the interplanar spacing of the reflecting atomic planes, one may choose a necessary frequency interval by simply rotating the crystal.

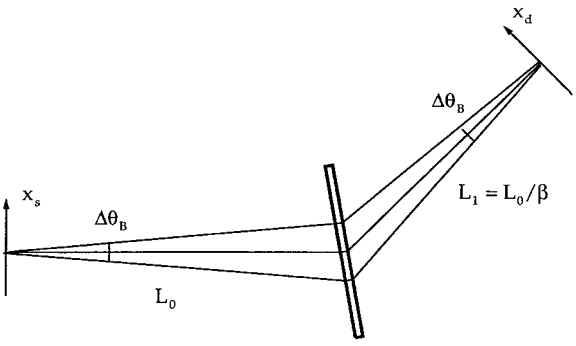

Fig. 3. Geometrical illustration of polychromatic focusing of the diffracted beam

2.4 Solution by Fourier transformation

The double integral in Eq. (13) may be reduced to a single integral by means of the Fourier transformation. We use a Fourier expansion of the propagators

$$P(x,L) = \int \frac{\mathrm{d}q}{2\pi} \exp(iqx)\, Q(q,L)\,,$$
$$G_h(x,d) = \int \frac{\mathrm{d}q}{2\pi} \exp(iqx)\, g_h(q,d)\,, \tag{15}$$

where

$$Q(q,L) = \int \mathrm{d}x \exp(-iqx)\, P(x,L) = \exp\left(-i\,\frac{\lambda L}{4\pi}\,q^2\right),$$
$$g_h(q,d) = \int \mathrm{d}x \exp(-iqx)\, G_h(x,d)\,. \tag{16}$$

Substituting Eq. (15) into Eq. (13) we obtain the expression

$$\tilde{\psi}(x_\mathrm{d},x_\mathrm{s}) = (\lambda L_\mathrm{t})^{1/2}\,\frac{1}{\beta}\int \frac{\mathrm{d}q}{2\pi} \exp\left(iq\left[x_\mathrm{d} - \frac{x_\mathrm{s}}{\beta}\right]\right) g_h(q\gamma_h,d_\mathrm{c}) \exp\left(-i\,\frac{\lambda\tilde{L}}{4\pi}\,q^2\right), \tag{17}$$

where $\tilde{L} = L_0/\beta^2 + L_1$.

This expression allows us to directly draw two conclusions. First, a shift of the point source in the source cross-section by Δx_s leads to a shift of the image pattern as a whole by $\Delta x_\mathrm{s}/\beta$ in the image plane. In this case the shift of the image does not depend on the distances. However, it depends on the asymmetry factor. A proper value of $\beta > 1$ leads to decreasing effective size of the source cross-section. This allows one to observe the coherent interference fringes. Second, the diffraction image depends on the effective distance $\tilde{L} = L_0/\beta^2 + L_1$ instead of the total distance $L_\mathrm{t} = L_0 + L_1$. Below we shall omit the coordinate x_s, considering $x_\mathrm{s} = 0$.

It is easy to obtain the Fourier transformation of the crystal propagator $g_h(q,d_\mathrm{c})$ as a solution of the Takagi equations with the boundary condition $E_0(x,0) = \exp(iqx)$. The solution is well known (see, for example, [22]). We write it as follows:

$$g_h(q\gamma_h,d_\mathrm{c}) = \sqrt{\beta}\left(\frac{\chi_h}{\chi_{\bar{h}}}\right)^{1/2}\frac{\exp(iA_0 - iqx_0)}{i\sqrt{\eta_\mathrm{c}^2+1}}\sin\left(\frac{K\sqrt{\chi_h\chi_{\bar{h}}}}{2\sqrt{\gamma_0\gamma_h}}\,d_\mathrm{c}\sqrt{\eta_\mathrm{c}^2+1}\right), \tag{18}$$

where $x_0 = d_\mathrm{c}\gamma_h(t_h - t_0)/2 = d_\mathrm{c}S_\mathrm{B}/2\gamma_0$,

$$A_0 = K\chi_0 d_\mathrm{c}\,\frac{(\beta+1)}{4\gamma_0}, \qquad \eta_\mathrm{c} = \frac{q}{K\sqrt{\chi_h\chi_{\bar{h}}}}\,\frac{S_\mathrm{B}}{\sqrt{\beta}} - \frac{\chi_0}{\sqrt{\chi_h\chi_{\bar{h}}}}\,\frac{(\beta-1)}{2\sqrt{\beta}}\,. \tag{19}$$

We note that $\eta_\mathrm{c} = \eta + i\eta_i$ is a complex value due to the fact that the parameters χ_0, χ_h, and $\chi_{\bar{h}}$ are complex values. Below we shall consider crystals having an inversion centre when $\chi_h = \chi_{\bar{h}}$ and take into account that $\chi_0 = -|\chi_{r0}| + i\chi_{i0}$, $\chi_h = -|\chi_{rh}| + i\chi_{ih}$, and $\chi_{i0,h} \ll |\chi_{r0,h}|$. Then we use a linear approximation over a parameter $\chi_{i0}/|\chi_{r0}|$ and obtain

$$\eta = \frac{S_\mathrm{B}}{\sqrt{\beta}}\,\frac{(q+q_0)}{K\,|\chi_{rh}|}, \qquad \eta_i = \frac{\chi_{i0}}{|\chi_{rh}|}\left(\varepsilon_h\,\eta - \frac{(\beta-1)}{2\sqrt{\beta}}\right), \tag{20}$$

where

$$q_0 = K\,|\chi_{r0}|\,\frac{(\beta-1)}{2S_{\mathrm{B}}}, \qquad \varepsilon_h = \frac{\chi_{ih}}{\chi_{i0}}\,. \tag{21}$$

For the purpose of a computer simulation of the image it is convenient to use a dimensionless variable η as the variable of integration. Thus, from Eq. (17) we may write the wave amplitude as

$$\tilde{\psi} = \frac{1}{2S_{\mathrm{B}}}\,\frac{(\lambda L_{\mathrm{t}})^{1/2}}{\Lambda\sqrt{\beta}}\int \frac{\mathrm{d}\eta}{\sqrt{\eta^2+1}}\sum_{\pm}(\pm 1)\exp\left[i\Phi_{\pm}(\eta) - M_{\pm}(\eta)\right], \tag{22}$$

where

$$\Phi_{\pm}(\eta) = \frac{\pi\alpha}{\Lambda}\,(x_{\mathrm{d}} - x_{\mathrm{C}})\,\eta - \frac{\pi d_0}{2\Lambda}\,\eta^2 + \Phi_{\pm}^{(0)}(\eta), \qquad \Phi_{\pm}^{(0)}(\eta) = \pm\frac{\pi d_{\mathrm{c}}}{\Lambda}\,\sqrt{\eta^2+1},$$

$$M_{\pm}(\eta) = \frac{\mu_0 d_{\mathrm{c}}}{2\sqrt{\gamma_0\gamma_h}}\left[\frac{(\beta+1)}{2\sqrt{\beta}} \mp \frac{\varepsilon_h}{\sqrt{\eta^2+1}} \mp \frac{\eta}{\sqrt{\eta^2+1}}\,\frac{(\beta-1)}{2\sqrt{\beta}}\right]. \tag{23}$$

Here we introduce the parameters

$$\Lambda = \frac{\lambda\sqrt{\gamma_0\gamma_h}}{|\chi_{rh}|}, \qquad d_0 = \frac{2\,|\chi_{rh}|\gamma_0}{S_{\mathrm{B}}^2\sqrt{\beta}}\left(\frac{L_0}{\beta} + L_1\beta\right),$$

$$\mu_0 = K\chi_{i0}\,, \qquad \alpha = \frac{2\gamma_0}{S_{\mathrm{B}}}\,, \qquad x_{\mathrm{C}} = x_0 - x_L\,, \qquad x_L = \frac{\lambda\tilde{L}}{2\pi}\,q_0\,. \tag{24}$$

The relative intensity is $I(x_{\mathrm{d}}) = |\tilde{\psi}(x_{\mathrm{d}})|^2$. The formulas (22) and (23) were used in a computer simulation of the relative intensity (see below). We note that in the symmetrical case of diffraction the formulas coincide with the formulas obtained earlier [15].

The upper sign corresponds to a slightly absorbing field which is just a candidate to be focused at the distance following from the condition $d_0(L_1) = d_{\mathrm{c}}$. In the experiment with a wedge-shaped crystal the distance is constant while the crystal thickness is varying. In this case the parameter d_0 is the thickness of the diffraction lens under the conditions of symmetrical diffraction. As is known, the real thickness of the crystal which corresponds to optimal focusing is a little larger than d_0. This is especially essential for asymmetrical diffraction. When absorption is negligible, one may observe interference fringes as a result of interference between two wave fields with different signs. Even if absorption is significant, interference is possible between different rays of the slightly absorbing field.

2.5 Method of computer simulation

The integral (22) may be calculated by means of the well-known fast Fourier transformation (FFT) procedure. However, there is another way to calculate the integral of a pure exponential function $\exp[f(\eta)]$ in finite limits where $f(\eta)$ may be a complex value:

$$\int_a^b \mathrm{d}\eta\exp\left[f(\eta)\right] = \sum_{n=1}^{N}\int_{a_n}^{b_n}\mathrm{d}\eta\exp\left[f(\eta)\right] \approx h\sum_{n=1}^{N}\frac{\exp\left[f(b_n)\right] - \exp\left[f(a_n)\right]}{f(b_n) - f(a_n)}\,, \tag{25}$$

where $a_1 = a$, $a_{n+1} = a_n + h = b_n$, and $h = (b - a)/N$. This method is convenient when the imaginary part of the argument $f(\eta)$ is a slowly varying function taking on large values. Then the interval is divided into a set of small intervals. Inside each small interval the argument is approximated as a linear function. In the case of the Fourier transformation when $f(\eta) = f_0(\eta) + i\eta x$, this algorithm may be optimized by preparing an array of values $\exp[f_0(a_n)]$ which is the same for all values of x while $\exp[i\eta a_n] = \exp[i\eta a_{n-1}] \exp[i\eta h]$.

2.6 Integral intensity

It is of interest to evaluate the integral intensity in the case when the detector has a wide window D. It measures the total intensity inside the window. In this case the integral relative intensity is

$$I_{\text{int}} = \frac{1}{D} \int_{x_C - D/2}^{x_C + D/2} \mathrm{d}x_d \, I(x_d) = \frac{\lambda L_t}{D(S_B \Lambda \beta)^2} \int \mathrm{d}\eta \, \mathrm{d}\eta' \, F(\eta) \, F^*(\eta')$$

$$\times \exp\left[-\frac{i\pi}{2\Lambda} \, d_0(\eta^2 - \eta'^2)\right] \int_{-D/2}^{+D/2} \mathrm{d}x'_d \exp\left(i \, \frac{\pi\alpha}{\Lambda}[\eta - \eta'] \, x'_d\right), \tag{26}$$

where

$$F(\eta) = \frac{\sqrt{\beta}}{2\sqrt{\eta^2 + 1}} \sum_{\pm} (\pm 1) \exp[i\Phi_{\pm}^{(0)}(\eta) - M_{\pm}(\eta)] \tag{27}$$

is an amplitude of reflection in the case of plane wave diffraction with the parameter η as a dimensionless parameter of the deviation from the Bragg condition.

When the width of the window is large enough to contain the whole peak of $I(x_d)$, one may replace the limits of integration over x_d by infinity. In this approximation the integral over x_d is equal to the Dirac delta function and the integral relative intensity is described by the equation

$$I_{\text{int}} = \frac{1}{\beta^2 \gamma_0 S_B} \, \frac{\lambda L_t}{\Lambda D} \int \mathrm{d}\eta \, |F(\eta)|^2 . \tag{28}$$

As follows from Eq. (28), the integral intensity in real space may be calculated as the integral intensity of plane waves with different values of the parameter of deviation from the Bragg condition. This fact is a consequence of Parseval's theorem.

We note that the result does not depend on the source cross-section size and the frequency bandwidth. However, a real intensity distribution depends on these parameters.

3. Analysis Based on the Stationary Phase Method

When $d_c \gg \Lambda$ or $d_0 \gg \Lambda$, the integrand of Eq. (22) is oscillating rapidly within the effective interval where its modulus has apparent values. In this case, the stationary phase method (see, for example, [23]) may be applied for an estimation of the integral

value. According to this method, for each value of the detector position x_d the small regions near the stationary phase points η_0 give significant contributions to the integral. Such a point η_0 is determined as a solution of the equation

$$\frac{d\Phi_\pm}{d\eta} = \frac{\pi}{\Lambda}\left[\alpha(x_d - x_C) - d_0\eta \pm d_c\frac{\eta}{\sqrt{\eta^2+1}}\right] = 0\,. \tag{29}$$

Then Eq. (22) may be replaced approximately by the expression

$$\tilde{\psi}(x_d) = \frac{\sqrt{2\pi}}{2S_B\sqrt{\beta}}\,\frac{(\lambda L_t)^{1/2}}{\Lambda}\sum_{\pm}(\pm 1)\sum_{\eta_0}\frac{\exp\left[i\Phi_\pm(\eta_0)\right]}{\left[\Phi''_\pm(\eta_0)\right]^{1/2}}\,\frac{\exp\left[-M_\pm(\eta_0)\right]}{\sqrt{\eta_0^2+1}}\,, \tag{30}$$

where $\Phi''_\pm = d^2\Phi_\pm/d\eta^2$. The sum includes all solutions of Eq. (29). In addition, different values of η_0 cannot be close to each other.

When $d_0 > 0$, the analytical solution of Eq. (29) is rather cumbersome. However, one may see that each value of η may be a point of stationary phase for the definite value of the detector position

$$x_d = x_C + U_\pm(\eta)\,, \qquad U_\pm(\eta) = \frac{\eta}{\alpha}\left[d_0 \mp \frac{d_c}{\sqrt{\eta^2+1}}\right]. \tag{31}$$

The solution may be obtained graphically in the plot (η, x) as the intersection point of the curve $[x_C + U(\eta)]$ with the line parallel to the η-axis at the height x_d. When d_0 is very large ($d_0 \gg d_c$), there is only one solution of Eq. (29) for both signs. The point of stationary phase $\eta = \alpha(x_d - x_C)/d_0$ is approximately the same for the two signs which correspond to the two branches of the dispersion surface in Ewald's theory [22]. In this case the intensity distribution reproduces the angular dependence of intensity in the theory of a plane incident wave. Therefore we may call the parameter η the angular parameter. In the general case, there is only one solution for the bottom sign in Eq. (29) for all values d_0 and d_c because the function $U_-(\eta)$ has a positive slope at all points. The same behavior takes place for the top sign if $d_c < d_0$.

When $d_c > d_0$, the curve $U_+(\eta)$ has a negative slope in the middle part of the η region where $d_0(\eta^2+1)^{1/2} < d_c$. In this region Eq. (29) has three solutions. Outside this region interference is possible only between waves of different branches of the dispersion surface. Inside this region a new kind of interference fringes is possible between different points of the same branch of the dispersion surface. There are two points $\eta_0 = \eta_f^{(1,2)}$ where $dU_+(\eta)/d\eta = 0$. At these points $\Phi''_+(\eta_0) = 0$. Therefore the solution (30) is not valid because it leads to an infinite intensity.

In a real situation the intensity is finite. However, it shows a sharp peak as a function of x_d because many rays go to the same point of the image. One may verify by means of an analysis in real space that this situation corresponds to the diffraction focus of the spherical wave. It is easy to calculate (see also [15]) that

$$\eta_f^{(1,2)} = \pm\left(\left(\frac{d_c}{d_0}\right)^{2/3} - 1\right)^{1/2}. \tag{32}$$

A substitution of (32) into (31) gives us an expression for the focus positions

$$x_{\mathrm{d}}^{(1,2)} = x_{\mathrm{C}} \mp \frac{d_0}{\alpha}\left(\left(\frac{d_{\mathrm{c}}}{d_0}\right)^{2/3} - 1\right)^{3/2}. \tag{33}$$

When $d_{\mathrm{c}} = d_0$, two focus positions coincide and correspond to a zero angular parameter $\eta_{\mathrm{f}}^{(1,2)} = 0$. Such a situation is beneficial in the symmetrical case ($\beta = 1$) because it corresponds to a maximum modulus of the slightly absorbing wave. A combination of the focus properties with the Borrmann effect gives the best result.

If the asymmetrical case is of interest ($\beta \neq 1$), we need to take into account the fact that the Borrmann effect is weakly pronounced, and the maximum modulus of the reflected wave corresponds to the angular parameter which is a solution of the equation $\mathrm{d}\tilde{M}_+(\eta)/\mathrm{d}\eta = 0$ where $\tilde{M}_+(\eta) = M_+(\eta) + (1/2)\log\left(\eta^2 + 1\right)$. We write this equation as

$$\eta = \frac{1}{\varepsilon_\beta + \varepsilon_\mu(\eta^2+1)^{1/2}\, d_0/d_{\mathrm{c}}}, \qquad \varepsilon_\beta = \frac{2\sqrt{\beta}\,\varepsilon_h}{(\beta-1)}, \qquad \varepsilon_\mu = \frac{4\gamma_0}{\mu_0 d_0}\,\frac{1}{(\beta-1)}. \tag{34}$$

The solution may be obtained graphically. It is easy to understand that the solution always has the same sign. When $\beta > 1$, it is always positive. Therefore in this case, only a focus with a positive η (when $x_{\mathrm{d}} < x_{\mathrm{C}}$) will have a significant intensity for $d_{\mathrm{c}} = d_{\mathrm{f}} > d_0$. The equation for $d_{\mathrm{f}} = d_0 r_{\mathrm{f}}$ may be obtained by substituting Eq. (32) into Eq. (34). It looks better for a dimensionless parameter r_{f} and may be written in the form

$$r_{\mathrm{f}}^{2/3} = 1 + \left(\varepsilon_\beta + \varepsilon_\mu r_{\mathrm{f}}^{-2/3}\right)^{-2}. \tag{35}$$

In the general case the equation is rather cumbersome. Let us assume that $r_{\mathrm{f}} = 1 + \varepsilon_{\mathrm{f}}$ and $\varepsilon_{\mathrm{f}} \ll 1$. Then the following expression for ε_{f} is approximately valid in a linear approximation:

$$\varepsilon_{\mathrm{f}} = \frac{1.5}{(\varepsilon_\mu + \varepsilon_\beta)^2 - 2\varepsilon_\mu/(\varepsilon_\mu + \varepsilon_\beta)}. \tag{36}$$

When the absorption is strong ($\varepsilon_\mu < 1$), the asymmetry parameter β cannot be large to obtain a small value of ε_{f}. In the case of large asymmetry ($\beta \gg 1$), absorption must be small to meet the condition $\varepsilon_\mu > 3$ while $\varepsilon_\beta \ll 1$. In this case $\varepsilon_{\mathrm{f}} = 1.5/(\varepsilon_\mu^2 - 2)$.

4. Usage of a Slit in Front of the Crystal

Let us now consider a more complicated case when the experimental setup includes a slit between the source and the crystal. The slit restricts only the x-dependence of the field. Therefore the y-dependence of the intensity stays the same, namely, it is absent. We need to consider only the x-dependence. In this section we shall use L_0 as the distance between the slit and the crystal, and we denote the distance between the source and the slit as L_{s} (see Fig. 4). As before, we first introduce the different optical trajectories for different relative frequencies θ_ω to satisfy the Bragg condition in the crystalline sample. Since the slit has the same position for all frequencies, the transverse position of the slit relative to the optical trajectories becomes different for different

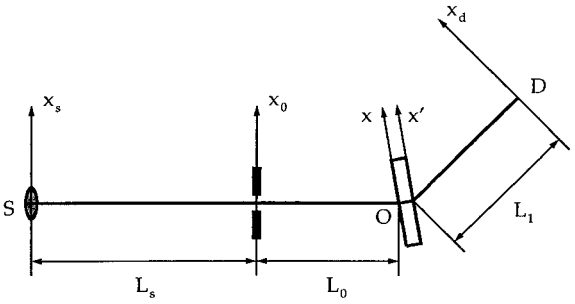

Fig. 4. Sketch of the experimental setup containing a slit between the source and the crystal plate

frequencies. It is shifted by the distance $x_{0\omega} = L_s\,\Delta\theta_B = -L_s \tan\theta_B \theta_\omega$. Let $2a$ be the slit width. Using the Huygens-Fresnel principle, we may consider each point of the slit as an intermediate source for which Eq. (17) is valid with x_0 instead of x_s and with $L'_t = L_s + L_t$ instead of $L_t = L_0 + L_1$. The real wave field is now described by the integral

$$\tilde{\psi}'(x_d, x_s) = \int_{x_{0\omega}-a}^{x_{0\omega}+a} dx_0\, \tilde{\psi}(x_d, x_0)\, P(x_0 - x_s, L_s)\,. \tag{37}$$

The formula is written for a definite relative frequency θ_ω in the local coordinate system. Let us introduce a new coordinate of the image $x'_d = x_d + x_{d\omega}$ independent of the frequency and take into account that now the distance betwen the source and the crystal is equal to $L_s + L_0$. Here $x_{d\omega} = ([L_s + L_0]/\beta - L_1) \tan\theta_B\, \theta_\omega$ (see Eq. (14)). We may rewrite Eq. (37) using the absolute coordinates of the image and the slit as

$$\tilde{\psi}'(x'_d, x_s, \theta_\omega) = \int_{-a}^{a} dx'_0\, \tilde{\psi}(x'_d - x_{d\omega}, x'_0 + x_{0\omega})\, P(x'_0 + x_{0\omega} - x_s, L_s)\,. \tag{38}$$

As follows from Eq. (17), the first and the second argument of the function $\tilde{\psi}$ are used in the combination $x'_d - x_{d\omega} - (x'_0 + x_{0\omega})/\beta = x'_d - x'_0/\beta - x'_{d\omega}$, where $x'_{d\omega} = x_{d\omega} + x_{0\omega}/\beta = (L_0/\beta - L_1) \tan\theta_B\, \theta_\omega$. Thus, we obtain the result that the condition for polychromatic focusing for the function $\tilde{\psi}$ is $L_0 = \beta L_1$, and this condition is independent of the distance L_s between the source and the slit. The relative intensity measured in an experiment with finite bandwidth may be written as

$$I(x'_d, x_s) = \frac{1}{2T_\omega} \int d\theta_\omega\, B(\theta_\omega)\, |\tilde{\psi}'(x'_d, x_s, \theta_\omega)|^2, \tag{39}$$

where $2T_\omega$ is the effective region of integration. Under the condition $L_0 = \beta L_1$ we obtain that $\tilde{\psi}$ does not depend on θ_ω and therefore

$$I(x'_d) = \int_{-a}^{a} dx'_0\, dx''_0\, \tilde{\psi}(x'_d, x'_0)\, \tilde{\psi}^*(x'_d, x''_0) \times \frac{1}{2T_\omega} \int d\theta_\omega\, B(\theta_\omega)\, P(x'_0 + x_{0\omega} - x_s, L_s)\, P^*(x''_0 + x_{0\omega} - x_s, L_s)\,. \tag{40}$$

The integral over θ_ω in this expression may be considered as a mutual coherence function for a slit due to a finite bandwidth of the source. Our aim is to show that for a large enough bandwidth this function is proportional to the Dirac delta function

$\delta(x_0' - x_0'')$. For example, for synchrotron radiation we may assume that $B(\theta_\omega) = \theta(T_\omega - |\theta_\omega|)$ where $\theta(x)$ is the Heaviside function. The effective region of integration $2T_\omega$ is defined by the longitudinal size of the crystal plate X_c and the distance L_0. Taking into account the definition made above, the integral over θ_ω is calculated as

$$\frac{1}{2T_\omega}\int \mathrm{d}\theta_\omega \cdots = P(x_0' - x_s, L_s)\, P^*(x_0'' - x_s, L_s)\, r\delta_r(x_0' - x_0'')\,, \tag{41}$$

where

$$\delta_r(x) = \frac{1}{\pi}\,\frac{\sin(\pi x/r)}{x} \xrightarrow[r\to 0]{} \delta(x)\,, \qquad r = \frac{\lambda}{2T_\omega \tan\theta_B}\,. \tag{42}$$

The function $\delta_r(x)$ has a sharp peak of width r. If the region of integration over θ_ω is large, so that r is much less than the width of the slit $2a$ as well as the characteristic range of other functions, then we may use the limit value of $\delta_r(x)$, namely, the Dirac delta function.

In such an approximation we obtain

$$I(x_d') = \frac{1}{2T_\omega L_s \tan\theta_B}\int_{-a}^{a} \mathrm{d}x_0'\, |\tilde{\psi}(x_d', x_0')|^2\,. \tag{43}$$

The physical meaning of this result is as follows. Under the conditions of polychromatic focusing for the distance from the slit to the crystal and for a wide bandwidth of radiation, the interference pattern is not influenced by the real source. On the other hand, the slit itself plays the role of a new incoherent source and the interference fringes must be averaged over the slit size. We note that the same result may be obtained when the source cross-section size is large and the distance L_s is small, as it was shown in the works [17, 24]. However, for synchrotron radiation the distance L_s is not small while the frequency bandwidth is large. As follows from Eq. (40), when we draw the optical axis through a point x_0 inside the slit, we obtain a new source position $x_s' = x_s - x_{0\omega}$. Even if the real source cross-section is small, the effective size becomes large for a large distance L_s and frequency bandwidth $2T_\omega$. This is the reason why we obtain the same result for synchrotron radiation.

We may evaluate the gain in this case as compared to the case of a large width of the slit when the slit is not essential. When $L_s \gg L_t$ and $|\tilde{\psi}|^2$ shows a gain of unity with L_t instead of L_t' (assuming the slit as a source), then Eq. (43) gives a gain of $g = a/(T_\omega L_t \tan\theta_B)$. For example, using the typical values $a = 20$ μm, $T_\omega = 10^{-2}$, and $L_t \tan\theta_B = 40$ cm, we obtain $g = 0.005$. Thus, experiments with a slit lead to a significant loss of intensity.

5. Specific Example: Interference Fringes of a New Kind

The experimental setup of synchrotron radiation beamlines of the third generation is characterized by a relatively small source cross-section size of about 30 μm and a long distance from the source to the object of about 40 m and longer. The distance behind the object cannot be that long. Therefore we have a situation where $L_0 \gg L_1$. To provide polychromatic focusing in this case, it is necessary to use asymmetrical diffraction with an asymmetry factor $\beta = L_0/L_1 \gg 1$. Let the angle between the internal normal to

the entrance surface $\mathbf{n}_0$ and the reciprocal lattice vector $\mathbf{h} = \mathbf{k}_h - \mathbf{k}_0$ be $\Psi = \pi/2 + \psi$. The angle ψ must be positive to obtain $\beta > 1$. Then $\varphi_0 = \theta_B - \psi$ and $\varphi_h = \theta_B + \psi$ where $\varphi_{0,h}$ are the angles between $\mathbf{k}_{0,h}$ and $\mathbf{n}_0$ (see Fig. 2). As is determined above, $\gamma_{0,h} = \cos\varphi_{0,h}$, $\beta = \gamma_0/\gamma_h$. The optimal condition arises when $\gamma_h \ll 1$ while $\gamma_0 \approx 1$. For a given value of the reciprocal lattice vector $\mathbf{h}$ and the direction of the unit vector $\mathbf{n}_0$ there is a critical value of the wavelength λ_c for which $\gamma_h = 0$. The parameter $\gamma_h > 0$ only for $\lambda < \lambda_c$. For cubic crystals $\lambda_c = 2d\left(1 - \cos^2\Psi\right)^{1/2}$, where $d = a\left(h^2 + k^2 + l^2\right)^{-1/2}$ and $\cos\Psi = (d/2\pi)(\mathbf{h}\mathbf{n}_0)$. Here a is the crystal lattice parameter and h, k, l are the Miller indices. When $\lambda_c - \lambda \ll \lambda$, the approximate relation $\gamma_h \approx (\lambda_c - \lambda)/[2d\,|\cos\Psi|]$ is valid.

As an example, we consider a silicon crystal plate ($a = 5.43$ Å) with an entrance surface normal to the (111) direction, a sample that is widely used in X-ray diffraction experiments. Taking into account that $\mathbf{n}_0 = -(1,1,1)/\sqrt{3}$, we have the relation $\cos\Psi = -(h + k + l)\,[3(h^2 + k^2 + l^2)]^{-1/2}$. We assume that the wedge-shaped sample has a side surface normal to the $(1\bar{1}0)$ direction. The scattering plane is normal to the $(11\bar{2})$ direction. Then, in order to realize asymmetrical diffraction, the Miller indices must have the values $(3\bar{1}1)$, (402), $(5\bar{1}2)$, $(7\bar{1}3)$, (804), and so on. We choose the case (804). This is of interest due to the large Bragg angle and the high energy of X-rays (low absorption). We consider an asymmetry factor $\beta = 25$ and distances $L_0 = 40$ m and $L_1 = 1.6$ m. This case is realized for X-rays having the wavelength $\lambda = 0.7308$ Å and the energy $E = 16.968$ keV, while the critical wavelength is $\lambda_c = 0.76792$ Å. Then we calculate $\sin\theta_B = 0.6019$ and $\cos\Psi = -0.775$. Since $\theta_B = 37^\circ < \psi$, both the incident and the diffracted wave lie on one side of the normal to the crystal surface, and $\varphi_0 = -13.77^\circ$ ($\gamma_0 = 0.971$) and $\varphi_h = 87.77^\circ$ ($\gamma_h = 0.039$). The parameters needed for a computer simulation are $\mu_0 = 0.001556\ \mu\text{m}^{-1}$, $\chi_{ih}/\chi_{i0} = 0.6637$, $|\chi_{r0}| = 3.371 \times 10^{-6}$, and $|\chi_{rh}| = 0.6057 \times 10^{-6}$.

The main geometrical directions for this case are shown explicitly in Fig. 5. The result of a direct computer simulation based on the theory developed above is shown in Fig. 6 as a two-dimensional map of intensity (topograph). The topograph of such a type may be registered experimentally with a wedge-shaped crystal sample. The values of intensity are related to the values of spherical wave intensity at the same distance from the source. This case is characterized by the parameters $\varepsilon_\beta = 0.277$ and $\varepsilon_\mu = 9.82$. The thickness of the crystal plate which focuses the X-ray spherical wave for the chosen parameters is rather small ($d_0 = 10.6$ μm and $\varepsilon_f = 0.015$), while the extinction length $\Lambda = 23.4$ μm. Therefore the diffraction focusing occurs for a very thin crystal, and it is not of practical interest. Also the region of "anomalous Pendellösung fringes" which was observed and discussed in [15] is absent here. For this reason, the topograph is "overexposed" to show the field of interference fringes of smaller intensity compared to the maximum intensity.

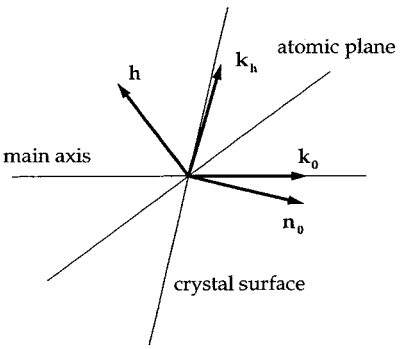

Fig. 5. Directions of the X-ray beam, the crystal surface, and the reciprocal lattice vector in the case of (804) diffraction in silicon with an asymmetry parameter $\beta = 25$

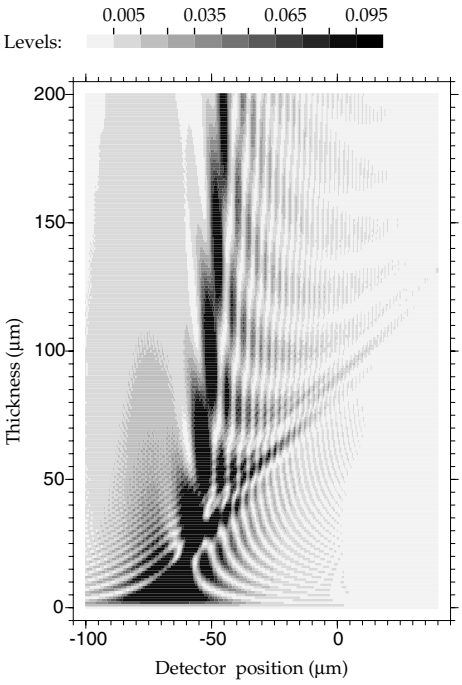

Fig. 6. Theoretical two-dimensional interference pattern obtained by a computer simulation for a wedge-shaped crystal in the case of (804) diffraction in silicon with an asymmetry parameter $\beta = 25$

Nevertheless, one may see the small region of "anomalous Pendellösung fringes" which is bounded by the region of quasi-focusing. The high asymmetry essentially decreases the focusing thickness of the crystal. Therefore the region of interference fringes similar to those observed by Kato and Lang [16] begins at small enough thicknesses of the crystal sample. This region is inclined in the asymmetrical case. The interference fringes having the shape of hyperbolas, corresponding to the interference of different branches of the dispersion surface, are presented only slightly. Such fringes were observed by Kato and Lang [16] and in other works (see [22]) in the symmetrical case only. A complete theory was presented in [25].

On the other hand, interference fringes of quite a new kind are well pronounced in the topograph. These fringes correspond to the interference of different parts of the same branch of the dispersion surface. These look like approximately vertical strips of intensity decreasing from the left to the right and were not observed previously. The origin of these fringes is more complicated. We note that the location of the main peak is $x_d^{(1)}$ (see Eq. (33)). The distance between the fringes is slightly varying. However, the distance between fringes far from the main peak is approximately the same.

Let us estimate this value analytically for small $|x_d| < \Lambda$ and $d_c \gg d_0, \Lambda$. As we pointed out before, the intensity is described approximately by Eq. (30), and only the upper sign and the positive roots are of interest. Equation (31) has two positive roots. One of them, η_1, is smaller than $\eta_f^{(1)}$ (see Eq. (32)). For the sake of simplicity we shall assume that $x_C < d_c/\alpha$ where α is determined by Eq. (24), and therefore $\eta_1 < 1$. For this root we obtain an approximate expression for the phase as $\Phi_1 \approx (\pi d_c/\Lambda)\,(1 - \eta_1^2/2)$. Here we took into account that $\eta_1 \approx \alpha(x_C - x_d)/d_c$. When $|x_d| \ll x_C$, we have $\Phi_1 \approx \text{const} + \pi(\alpha^2 x_C/\Lambda d_c)\, x_d$. The position dependence of the phase Φ_1 is weak under the conditions we assume. The second root η_2, on the contrary, is much larger than $\eta_f^{(1)}$ and $\eta_2 \gg 1$. Therefore the phase is determined approximately as $\Phi_2 \approx (\pi d_0/2\Lambda)\,\eta_2^2 \approx \pi(\alpha^2 x_L/\Lambda d_0)\, x_d$. Here we used the relation $\eta_2 \approx \alpha(x_d + x_L)/d_0$ where x_L is determined by Eq. (24). We took into account that $\alpha x_0 = d_c$. When $x_L \gg d_0$, this phase may change significantly.

Hence we may conclude that the intensity is varying due to the change of the phase Φ_2 only, and the distance p_f between fringes is determined from the relation $\Delta\Phi_2 = 2\pi$.

As a result, we obtain $p_f = 2\Lambda d_0/\alpha^2 x_L$. For our specific case this estimation gives $p_f = 1.7$ μm, which is in good agreement with the numerical results. We note that for high asymmetry ($\beta \gg 1$) the distance depends on β as $p_f \propto \beta^{-2}$, because $\Lambda \propto 1/\sqrt{\beta}$, $d_0 \propto 1/\sqrt{\beta}$, and $x_L \propto \beta$ (see Eq. (24)). On the other hand, in the first approximation it is independent of the crystal thickness.

6. Conclusion

We developed a consistent theory of X-ray spherical wave dynamical diffraction in a perfect crystal taking into account the distances in front of and behind the crystal. The general case of asymmetrical diffraction is considered for the first time. The perfect crystal influences the plane wave components of the Fourier expansion of the spherical wave. As a result, the spherical wave is transformed into a wave of varying intensity that allows one to speak about the perfect crystal imaging. The image of the perfect crystal depends on the crystal parameters as well as the distances in air. The image looks like an interference pattern where the intensity oscillates due to the interference of different plane wave components having different phases. The initial formulas were obtained by the technique of propagators. This also allows us to estimate the role of the slit which may be installed between the X-ray source and the crystal.

We analyzed the role of finite frequency bandwidth and transverse X-ray source cross-section size. It was shown that in the case of asymmetrical diffraction with a high level of the asymmetry parameter β the different frequencies lead to the same position of the interference pattern (polychromatic focusing) when the distance from the source to the crystal is β times larger than the distance from the crystal to the detector. The finite source cross-section size leads to smoothing of the interference pattern over a region which is β times smaller than the source size. This is why the asymmetrical case of diffraction may be of interest for experiments with synchrotron radiation sources of the third generation, taking into account that the distance from the source to the crystal is about 40 m and more, while the distance from the crystal to the detector cannot be larger than 5 m. Usage of a narrow slit allows one to investigate symmetrical diffraction with synchrotron radiation. Under the conditions of polychromatic focusing the slit plays the role of a new incoherent X-ray source.

Highly asymmetrical diffraction is characterized by small crystal thickness of diffraction spherical wave focusing. On the other hand, it leads to interference fringes of a new kind, which were not observed previously. These fringes are formed by interference of plane wave components which correspond to the same branch of the dispersion surface. The distance between the intensity peaks decreases with increasing β as $1/\beta^2$, and it is practically independent of the crystal thickness. This new interference phenomenon may be used for an estimation of the effective source size of a synchrotron source.

References

[1] V. A. SOMENKOV, A. K. TKALICH, and S. S. SHILSTEIN, J. Tech. Phys. **61**, 197 (1991).
[2] V. N. INGAL and E. A. BELIAEVSKAYA, J. Phys. D **28**, 2314 (1995).
[3] T. J. DAVIS, T. E. GUREYEV, D. GAO, A. W. STEVENSON, and S. W. WILKINS, Phys. Rev. Lett. **74**, 3173 (1995).
[4] T. E. GUREYEV and S. W. WILKINS, Il Nuovo Cimento **19D**, 545 (1997).

[5] A. Snigirev, I. Snigireva, V. Kohn, S. Kuznetsov, and I. Schelokov, Rev. Sci. Instrum. **66**, 5486 (1995).
[6] P. Cloetens, R. Barrett, J. Baruchel, J. P. Guigay, and M. Schlenker, J. Phys. D **29**, 133 (1996).
[7] S. W. Wilkins, T. E. Gureyev, D. Gao, A. Pogany, and A. W. Stevenson, Nature **384**, 335 (1996).
[8] G. Margaritondo and G. Tromba, J. Appl. Phys. **85**, 3406 (1999).
[9] A. Snigirev, V. Kohn, I. Snigireva, and B. Lengeler, Nature **384**, 49 (1996).
[10] P. Elleaume, J. Synchrotron Radiat. **5**, 1 (1998).
[11] B. Lengeler, C. G. Schroer, M. Richwin, J. Tummler, M. Drakopoulos, A. Snigirev, and I. Snigireva, Appl. Phys. Lett. **74**, 3924 (1999).
[12] V. Mocella, J. P. Guigay, Y. Epelboin, J. Hartwig, J. Baruchel, and A. Mazuelas, J. Phys. D **32**, A88 (1999).
[13] A. M. Afanasev and V. G. Kohn, Soviet Phys. – Solid State **19**, 1035 (1977).
[14] V. V. Aristov, V. I. Polovinkina, I. M. Shmytko, and E. V. Shulakov, Soviet Phys. – JETP Lett. **28**, 6 (1978).
[15] V. V. Aristov, V. I. Polovinkina, A. M. Afanasev, and V. G. Kohn, Acta Cryst. **A36**, 1002 (1980).
[16] N. Kato and A. R. Lang, Acta Cryst. **12**, 787 (1959).
[17] V. V. Aristov, A. A. Snigirev, A. M. Afanasev, V. G. Kohn, and V. I. Polovinkina, Acta Cryst. **A42**, 426 (1986).
[18] S. Takagi, Acta Cryst. **15**, 1311 (1962).
[19] S. Takagi, J. Phys. Soc. Jpn. **26**, 1239 (1968).
[20] A. M. Afanasev and V. G. Kohn, Acta Cryst. **A27**, 421 (1971).
[21] J. Cowley, Diffraction Physics, North-Holland Publ. Co., Amsterdam 1975.
[22] Z. G. Pinsker, Dynamical Scattering of X-Rays in Crystals, Springer-Verlag, Berlin/Heidelberg/New York 1984.
[23] H. Jeffreys and B. Swirles, Methods of Mathematical Physics, Cambridge University Press, Cambridge 1966.
[24] V. V. Aristov, V. G. Kohn, V. I. Polovinkina, and A. A. Snigirev, phys. stat. sol. (a) **72**, 483 (1982).
[25] N. Kato, J. Appl. Phys. **39**, 2225 (1968).